Chinese Journal of Natural Medicines

**Amoenucles AF, novel nucleoside derivatives with TNF-α inhibitory activities from *Aspergillus amoenus* TJ507**

Yeting Zhang, Zhengyi Shi, Chunhua Zhao, Lanqin Li, Ming Chen, Yunfang Cao, Fengqing Wang, Bo Tao, Xinye Huang, Jieru Guo, Changxing Qi, Weiguang Sun, Yonghui Zhang

**Citation:** Yeting Zhang, Zhengyi Shi, Chunhua Zhao, Lanqin Li, Ming Chen, Yunfang Cao, Fengqing Wang, Bo Tao, Xinye Huang, Jieru Guo, Changxing Qi, Weiguang Sun, Yonghui Zhang, Amoenucles AF, novel nucleoside derivatives with TNF-α inhibitory activities from *Aspergillus amoenus* TJ507, Chinese Journal of Natural Medicines, 2025, 23(1), 111-118. doi: 10.1016/S1875-5364(25)60805-3.

View online: https://doi.org/10.1016/S1875-5364(25)60805-3

Chinese Journal of Natural Medicines 23 (2025) 111-118

Contents lists available at ScienceDirect

Chinese Journal of Natural Medicines

journal homepage: www.cjnmcpu.com/

Original article

# Amoenucles A–F, novel nucleoside derivatives with TNF-α inhibitory activities from *Aspergillus amoenus* TJ507

Yeting Zhang[a,Δ], Zhengyi Shi[a,Δ], Chunhua Zhao[a,Δ], Lanqin Li[a], Ming Chen[a], Yunfang Cao[a], Fengqing Wang[a], Bo Tao[a], Xinye Huang[a], Jieru Guo[c,*], Changxing Qi[a,b,*], Weiguang Sun[a,*], Yonghui Zhang[a,*]

[a] *Hubei Key Laboratory of Natural Medicinal Chemistry and Resource Evaluation, School of Pharmacy, Tongji Medical College, Huazhong University of Science and Technology, Wuhan 430030, China*

[b] *Institute of Organ Transplantation, Tongji Hospital, Tongji Medical College, Huazhong University of Science and Technology, Key Laboratory of Organ Transplantation, Ministry of Education, NHC Key Laboratory of Organ Transplantation, Chinese Academy of Medical Sciences, Wuhan 430030, China*

[c] *Department of Pharmacy, Tongji Hospital, Tongji Medical college, Huazhong University of Science and Technology, Wuhan 430033, China*

ARTICLE INFO

*Article history:*
Received 1 February 2024
Revised 4 May 2024
Accepted 14 June 2024
Available online 20 January 2025

*Keywords:*
*Aspergillus amoenus* TJ507
Nucleoside derivatives
Intramolecular transesterification
Tumor necrosis factor α (TNF-α)

ABSTRACT

Amoenucles A–F (**1**–**6**), six previously undescribed nucleoside derivatives, and two known analogs (**7** and **8**) were isolated from the culture of *Aspergillus amoenus* TJ507. Their structures were elucidated through spectroscopic analysis, single-crystal X-ray crystallography, and chemical reactions. Notably, **3** and **4** represent the first reported instances of nucleosides with an attached pyrrole moiety. Of particular significance, the absolute configuration of the sugar moiety of **1**–**4** was determined using nuclear magnetic resonance (NMR), electric circular dichroism (ECD) calculations, and a hydrolysis reaction, presenting a potentially valuable method for confirming nucleoside structures. Furthermore, **1**, **2**, and **5**–**8** exhibited potential tumor necrosis factor α (TNF-α) inhibitory activities, which may provide a novel chemical template for the development of agents targeting autoimmune and inflammatory diseases.

## 1. Introduction

Nucleosides, comprised of a sugar moiety and nucleobase, play a widespread role in the synthesis of DNA and RNA during cellular processes [1, 2]. Nucleoside derivatives have significant importance in medicinal chemistry, with several finding clinical applications as antiviral drugs (e.g., zidovudine, lamivudine, and vidarabine) and antitumor agents (e.g., cytarabine) [3, 4]. Natural nucleosides serve as a crucial source of clinical drugs and bioactive molecules [5-9]. For instance, A-94964, a uridine-containing natural nucleoside isolated from *Streptomyces* sp., functions as an inhibitor of bacterial translocase 1 [10]. Consequently, the discovery of novel natural nucleoside derivatives remains essential in addressing global health challenges.

Natural products derived from microorganisms have been recognized as an essential source of drugs or lead compounds, including penicillin [11], erythromycin, and lovastatin [8, 12-16]. In our ongoing research to discover structurally complex and bioactive metabolites from fungi [17-21], six previously undescribed nucleoside derivatives, named amoenucles A–F (**1**–**6**), along with two known congeners, kipukasin D (**7**) and kipukasin E (**8**) (Fig. 1), were isolated from the culture of *Aspergillus amoenus* TJ507. Compounds **3** and **4** represent the first examples of nucleoside derivatives with an attached pyrrole moiety. Notably, compounds **1**, **2**, and **5**–**8** exhibited moderate tumor necrosis factor α (TNF-α) inhibitory activities, with $IC_{50}$ values ranging from (8.95 ± 0.62) to (17.70 ± 1.40) μmol·L$^{-1}$. This study marks the first report of nucleosides serving as TNF-α inhibitors, potentially providing new chemical scaffolds for research into treatments for autoimmune and inflammatory diseases. This paper presents the isolation, structure elucidation, and bioactivity tests of compounds **1**–**8**.

## 2. Result and discussion

Amoenucle A (**1**) has the molecular formula $C_{20}H_{24}N_2O_8$, corresponding to ten degrees of unsaturation, as determined by high-resolution electrospray ionization mass spectrometry (HR-ESI-MS) data. The $^1$H nuclear magnetic resonance (NMR) spectrum (Table 1) exhibited signals for three olefinic protons ($\delta_H$ 7.87 d, $J$ = 1.2 Hz; 6.43 d, $J$ = 2.2 Hz; 6.40 d, $J$ = 2.2 Hz), three oxymethine protons ($\delta_H$ 6.34 dd, $J$ = 8.6, 5.8 Hz; 5.51 dt, $J$ = 5.7 Hz, 1.7Hz; 4.20 q, $J$ = 3.1 Hz), two methylene units (one oxygenated) ($\delta_H$ 3.86 d, $J$ = 3.1 Hz), and four methyl groups (two oxygenated) ($\delta_H$ 1.90 d, $J$ = 1.2 Hz; 3.83 s; 3.81 s; 2.28 s). The $^{13}$C NMR and distortionless enhancement by polarization transfer (DEPT) spectra (Table 2) indicated the presence of three carboxy or amide carbons ($\delta_C$ 169.5; 166.3; 152.4) and one olefinic carbon. Overall, the NMR

* Corresponding author.
*E-mail addresses:* guojieru314@163.com (J. Guo); qichangxing@hust.edu.cn (C. Qi); weiguang_sun@hust.edu.cn (W. Sun); zhangyh@mails.tjmu.edu.cn (Y. Zhang)

Δ These authors contributed equally to this work.

https://doi.org/10.1016/S1875-5364(25)60805-3

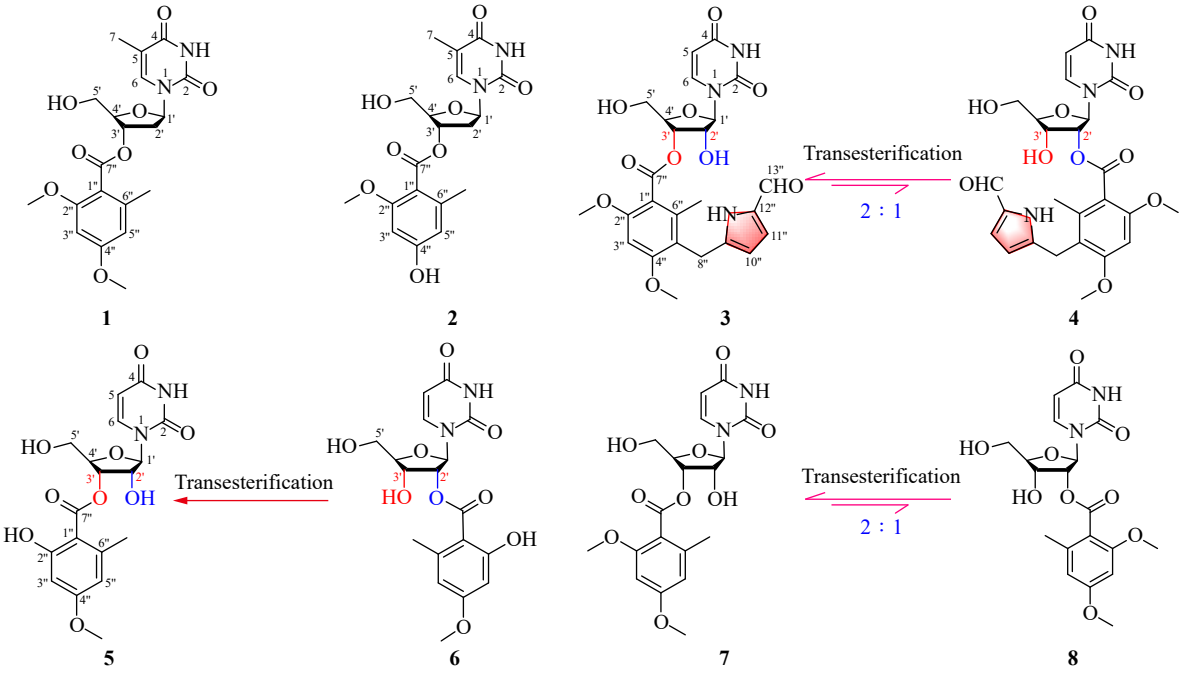


**Fig. 1** Structures of compounds **1**–**8**.

**Table 1** $^{1}$H NMR data of **1**–**6** recorded in $CD_3OD$ (mult, *J* in Hz).

| No. | **1**[a] | **2**[a] | **3**[b] | **4**[b] | **5**[b] | **6**[b] |
|---|---|---|---|---|---|---|
| 5 | | | 5.75 d (8.1) | 5.76 d (8.1) | 5.69 d (8.1) | 5.75 d (8.1) |
| 6 | 7.87 d (1.2) | 7.88 d (1.2) | 8.00 d (8.1) | 8.03 d (8.1) | 8.01 d (8.1) | 8.03 d (8.1) |
| 7 | 1.90 d (1.2) | 1.90 d (1.2) | | | | |
| 1′ | 6.34 dd (8.6, 5.8) | 6.35 dd (8.6, 5.8) | 5.99 d (6.6) | 6.18 d (5.5) | 5.90 d (4.7) | 6.05 d (6.1) |
| 2′ | 2.41 dd (8.6, 5.7)<br>2.44 dd (5.8, 2.1) | 2.40 dd (8.6, 5.7)<br>2.44 dd (5.9, 2.1) | 4.52 dd (6.6, 5.5) | 5.50 t (5.5) | 4.18 t (5.0) | 4.57 t (5.8) |
| 3′ | 5.51 dt (5.7, 1.7) | 5.50 dt (5.7, 1.7) | 5.39 dd (5.5, 3.1) | 4.47 dd (5.5, 4.4) | 4.15 t (5.0) | 5.50 t (5.4) |
| 4′ | 4.20 q (3.1) | 4.20 q (3.1) | 4.26 q (2.7) | 4.03 q (2.9) | 4.00 dt (4.7, 2.9) | 4.32 q (2.8) |
| 5′ | 3.86 d (3.1) | 3.86 d (3.1) | 3.84 dd (12.3, 3.1) | 3.76 dd (12.3, 3.1) | 3.73 dd (12.3, 3.2) | 3.73 dd (12.3, 3.2) |
| | | | 3.85 dd (12.3, 2.9) | 3.79 dd (12.3, 2.9) | 3.85 dd (12.3, 2.7) | 3.85 dd (12.3, 2.7) |
| 3″ | 6.43 d (2.2) | 6.31 d (2.2) | 6.63 s | 6.60 s | 6.31 d (2.6) | 6.34 d (2.6) |
| 5″ | 6.40 d (2.2) | 6.26 d (2.2) | | | 6.33 d (2.6) | 6.36 d (2.6) |
| 8″ | | | 4.00 s | 3.99 s | | |
| 10″ | | | 5.80 d (3.9) | 5.78 d (4.0) | | |
| 11″ | | | 6.89 d (3.9) | 6.88 d (4.0) | | |
| 13″ | | | 9.24 s | 9.24 s | | |
| 2″-$OCH_3$ | 3.83 s | 3.79 s | 3.89 s | 3.84 s | | |
| 4″-$OCH_3$ | 3.81 s | | 3.90 s | 3.88 s | 3.79 s | 3.80 s |
| 6″-$CH_3$ | 2.28 s | 2.23 s | 2.24 s | 2.20 s | 2.48 s | 2.59 s |

[a] $^{1}$H NMR 400 MHz; [b] $^{1}$H NMR 600 MHz.

data of **1** closely resembled that of the known compound kipukasin D (**7**) [22].

The primary distinction between **1** and **7** was the presence of a methyl group ($\delta_H$ 1.90 d, *J* = 1.2 Hz) attached at C-5 in **1**, as evidenced by the heteronuclear multiple bond correlation (HMBC) cross-peaks from $H_3$-7 to C-4, C-5, and C-6. Furthermore, the $^{1}$H–$^{1}$H correlation spectroscopy (COSY) correlations of H-1′/$H_2$-2′/H-3′/H-4′/$H_2$-5′ and the chemical shift of C-2′ ($\delta_C$ 38.5) confirmed the thymidine moiety of **1** (Fig. S1). The attachment of the 2,4-dimethoxy-6-methyl benzoic acid unit to C-3′ was determined through analyses of 1D and 2D NMR spectra and comparison of the NMR data of **1** with those of **7**.

**Table 2** $^{13}C$ NMR data of **1**–**6** recorded in $CD_3OD$.

| No. | **1**[a] | **2**[a] | **3**[b] | **4**[b] | **5**[b] | **6**[b] |
|---|---|---|---|---|---|---|
| 2 | 152.4 | 152.4 | 152.6 | 152.2 | 152.5 | 152.5 |
| 4 | 166.3 | 166.4 | 166.1 | 166.1 | 166.2 | 166.0 |
| 5 | 111.9 | 111.9 | 103.2 | 103.1 | 102.6 | 103.2 |
| 5-$CH_3$ | 12.5 | 12.5 | | | | |
| 6 | 137.9 | 137.9 | 142.5 | 142.8 | 142.7 | 142.4 |
| 1′ | 86.2 | 86.2 | 89.8 | 88.3 | 90.7 | 90.4 |
| 2′ | 38.5 | 38.5 | 74.1 | 77.1 | 75.7 | 74.0 |
| 3′ | 77.1 | 77.0 | 75.0 | 70.6 | 71.3 | 75.1 |
| 4′ | 86.5 | 86.5 | 84.8 | 87.0 | 86.4 | 84.6 |
| 5′ | 63.1 | 63.1 | 62.5 | 62.3 | 62.3 | 62.4 |
| 1″ | 116.5 | 115.0 | 117.4 | 117.2 | 107.0 | 107.0 |
| 2″ | 160.2 | 160.5 | 158.5 | 158.5 | 165.4 | 165.4 |
| 3″ | 97.1 | 97.8 | 94.6 | 94.6 | 99.7 | 99.9 |
| 4″ | 163.5 | 161.5 | 161.1 | 161.1 | 165.9 | 165.4 |
| 5″ | 108.1 | 110.2 | 118.7 | 118.6 | 111.6 | 111.7 |
| 6″ | 139.6 | 139.8 | 137.7 | 137.6 | 144.1 | 144.6 |
| 7″ | 169.5 | 169.7 | 169.7 | 169.4 | 173.4 | 173.3 |
| 8″ | | | 24.8 | 24.8 | | |
| 9″ | | | 143.9 | 144.0 | | |
| 10″ | | | 110.6 | 110.5 | | |
| 11″ | | | 124.9 | 124.7 | | |
| 12″ | | | 133.2 | 133.0 | | |
| 13″ | | | 179.8 | 179.8 | | |
| 2″-$OCH_3$ | 56.4 | 56.3 | 56.7 | 56.6 | | |
| 4″-$OCH_3$ | 55.9 | | 56.4 | 56.4 | 55.8 | 55.8 |
| 6″-$CH_3$ | 19.9 | 19.9 | 16.8 | 16.8 | 24.1 | 24.4 |

[a] $^{13}C$ NMR 100 MHz; [b] $^{13}C$ NMR 150 MHz.

Furthermore, the relative configuration of the sugar moiety in **1** was elucidated using nuclear overhauser effect spectroscopy (NOESY) spectroscopy. The observed correlation between H-1′ and H-4′ indicated their presence on the same face, while the key nuclear overhauser effect (NOE) correlation of H-3′ and H-5′ suggested their positioning on the same side (Fig. S2). To determine the absolute configuration of **1**, electric circular dichroism (ECD) calculations based on time-dependent density functional theory (TD-DFT) were employed (Fig. 2). Additionally, compound **1** underwent a hydrolysis reaction. The retention time, $^1H$ NMR data, and circular dichroism (CD) spectrum of the nucleoside component of the reaction product (**1a**) were identical to those of thymine-1-*β*-D-deoxyribofuranoside under the same conditions (Figs. 3, 4 and Supporting Information). These findings collectively confirmed the configuration of the sugar moiety in **1**.

Amoenucle B (**2**) exhibited a molecular formula of $C_{19}H_{22}N_2O_8$ based on its HR-ESI-MS data. The $^1H$ and $^{13}C$ NMR spectral data (Tables 1 and 2) revealed three olefin protons ($\delta_H$ 7.88 d, $J$ = 1.2Hz; 6.31 d, $J$ = 2.2 Hz; 6.26 d, $J$ = 2.2 Hz), three oxymethine protons ($\delta_H$ 6.35 dd, $J$ = 8.6, 5.8 Hz; 5.50 dt, $J$ = 5.7, 1.7 Hz; 4.20 q, $J$ = 3.1 Hz), two methylene units (one oxygenated) ($\delta_H$ 3.86 d, $J$ = 3.1 Hz) and three methyl ($\delta_H$ 1.90 d, $J$ = 1.2 Hz; 3.79 s; 2.23 s) (one oxygenated) protons. These data were comparable to compound **1**, with the notable difference being a hydroxyl group attached to C-4″ in **2** instead of a methoxy substituent on C-4″ in **1**. This distinction was confirmed by the molecular formula and the upfield shift of the C-4″ resonance ($\delta_C$ 161.5). Consequently, the planar structure of **2** was elucidated.

The relative configuration of **2** was determined through analysis of NOESY data. NOESY cross-peaks observed between H-1′/H-4′ indicated the same orientation for these protons. Additionally, H-3′ and H-5′ were positioned on the same face, as evidenced by the between H-3′ and H-5′ (Fig. S2). The absolute configuration was presumed to be identical to that of **1**, based on the consistency of chemical shifts in the deoxyribose moiety of **2** with those of **1**, and the close match between the experimental ECD spectrum of **2** and both the experimental and calculated ECD spectra of **1** (Fig. 2). Furthermore, the nucleoside portion was conclusively verified through hydrolysis reaction and subsequent comparison of retention time (Fig. 4), NMR data, and CD spectra with thymine-1-*β*-D-deoxyribofuranoside (Fig. 5 and Supporting Information).

Amoenucles C (**3**) and D (**4**) exhibited a molecular formula of $C_{25}H_{27}N_3O_{10}$ based on HR-ESI-MS data with a positive molecular ion at $m/z$ 552.1609 $[M + Na]^+$ (Calcd. for $C_{25}H_{27}N_3O_{10}Na$, 552.1594). The $^1H$ NMR and $^{13}C$ NMR (Tables 1 and 2) chemical

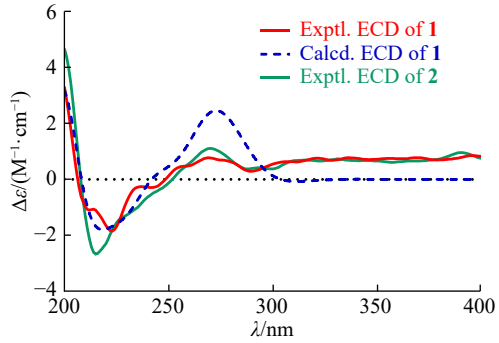


**Fig. 2** Experimental and calculated ECD spectra of **1** and experimental ECD spectra of **2**.

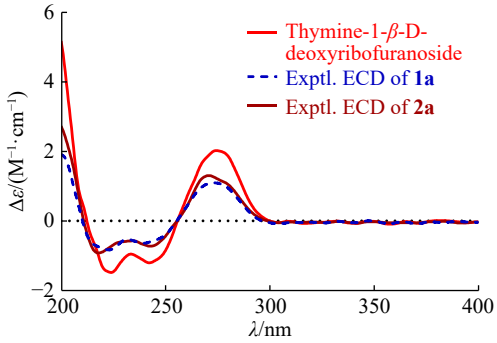


**Fig. 3** CD spectra of thymine-1-*β*-D-deoxyribofuranoside and hydrolysates of **1** and **2**.

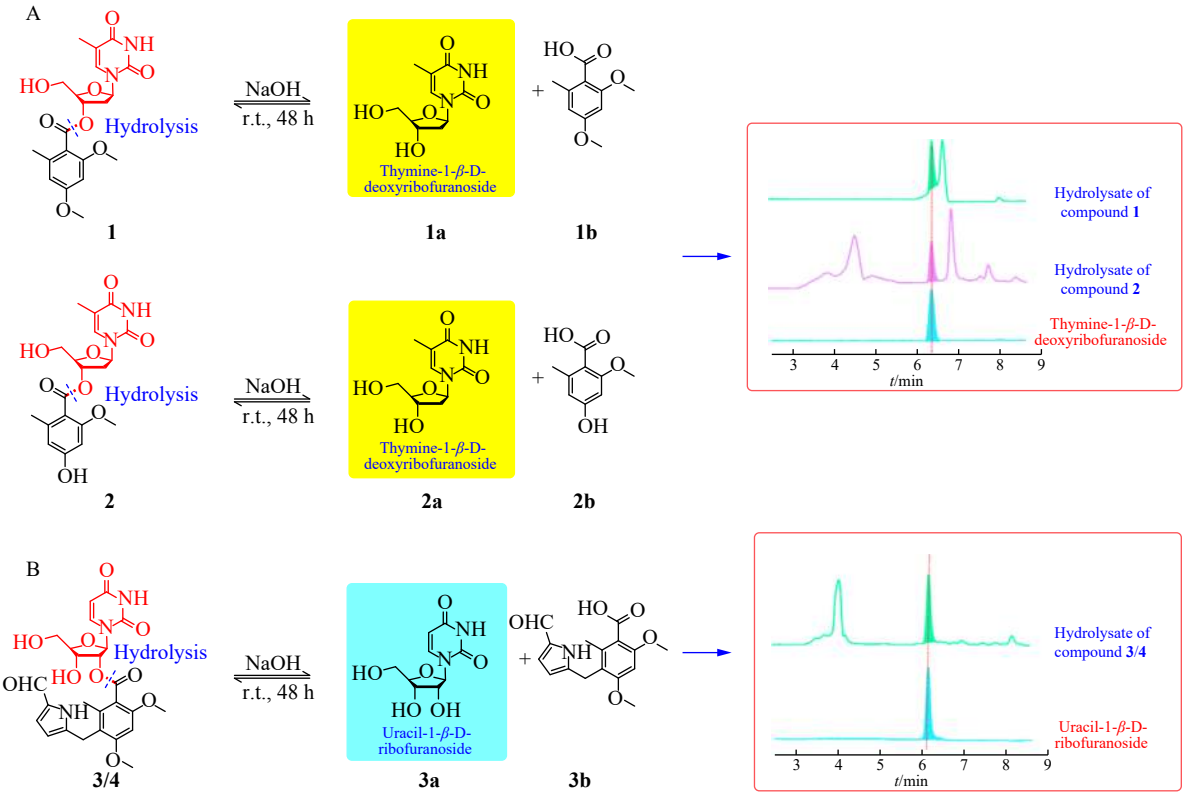


**Fig. 4** Stereochemical determination of **1** and **2** (A), **3**/**4** (B) by hydrolysis and high-performance liquid chromatography (HPLC) analysis.

shift assignments revealed two sets of compounds **3** and **4** with an approximate ratio of 2∶1. Initially, compounds **3** and **4** were separated through HPLC using reversed-phase (RP) $C_{18}$. However, compounds **3** and **4** rapidly rearranged at room temperature, ultimately maintaining a 2∶1 ratio after 48 h (Fig. S2). This phenomenon, termed 2′/3′-transesterification, has been observed in the known compounds kipukasin D (**7**) and kipukasin E (**8**) and has been reported to occur in some nucleoside derivatives [23].

The primary component (**3**) exhibited similarities to the corresponding signals of kipukasin D (**7**), with the main distinction between **3** and **7** observed in the substituent moiety at C-5″. Compound **3** featured an additional pyrrole moiety attached at C-5″, as evidenced by the HMBC correlation from $H_2$-8″ to C-4″, C-5″, C-6″, C-9″, and C-10″; from H-11″ to C-12″ and C-13″, along with the $^1$H–$^1$H COSY signal between H-10″ and H-11″ (Fig. S1). These findings elucidated the planar structure of **3**. Similar to **7**/**8**, amoenucles D (**3**) and E (**4**) were identified as a pair of regioisomers based on their mixed NMR spectra. Compound **4** closely resembled **3**, differing only in the exchange of substituents between C-2′ and C-3′. Comprehensive analysis of the NMR spectra confirmed the planar structure of **4**, as evidenced by the subtle signal differences for H-2′ ($\delta_H$ 5.50; t, $J$ = 5.4 Hz) and the H-3′ resonance ($\delta_H$ 4.47; dd, $J$ = 5.4 and 4.4 Hz) (Table 1). Furthermore, the HMBC correlation from H-2′ to C-7″ supported this connection for **4** (Fig. S1).

The NOESY spectra of **3** and **4** exhibited correlations between H-1′ and H-4′, confirming their presence on the same face. Additionally, cross-peaks observed in H-2′/H-3′/H-5′ indicated these protons shared the same orientation (Fig. S2). Based on biogenetic considerations and hydrolysis reactions, the retention time and NMR data of the hydrolysate (**3a**) of **3**/**4** were analyzed and found to be identical to that of uracil-1-*β*-D-ribofuranoside (Fig. 4). Furthermore, the CD spectra of the hydrolysate of **3**/**4** aligned with the standard of uracil-1-*β*-D-ribofuranoside, determining the absolute configuration of the nucleoside portion of **3** as 1′*R*,2′*R*,3′*S*,4′*R* and **4** as 1′*R*,2′*R*,3′*R*,4′*R* (Fig. 5).

Amoenucles A (**5**) and B (**6**) were determined to have the

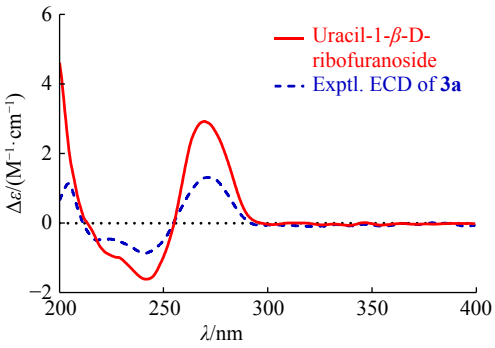


**Fig. 5** CD spectra of uracil-1-$\beta$-D-ribofuranoside and hydrolysate of **3/4**.

identical molecular formula $C_{18}H_{20}N_2O_9$, suggesting 10 degrees of unsaturation, based on HR-ESI-MS data of the inseparable mixture showing a sodium ion peak at $m/z$ 431.1050 $[M + Na]^+$ (Calcd. for $C_{18}H_{20}N_2O_9Na$, 431.1066). The IR spectrum of **5** displayed absorption bands for the hydroxyl group (3423 $cm^{-1}$) and carbonyl group (1690 $cm^{-1}$). The 1D NMR spectra revealed two sets of signals for compounds **5** and **6**, and a detailed analysis of their NMR data disclosed they were nucleoside derivatives. Interestingly, the integration of the mixed $^1H$ NMR displayed two sets of compounds **5** and **6** with a ratio of 1∶2, while $^{13}C$ NMR indicated a ratio of 3∶1 for **5** and **6**. To identify the transesterification ratio of **5/6**, we reanalyzed the mixed compounds by HPLC using RP-$C_{18}$. Unexpectedly, only a single peak was observed, and the spectrum of the peak demonstrated that compound **6** could fully convert to **5**. Subsequently, we obtained purified spectra and a suitable crystal of **5**.

The purified $^{13}C$ NMR spectrum (Table 2) of the main component (**5**) revealed 18 carbon signals, including three carbonyl carbons ($\delta_C$ 152.5, 166.2 and 173.4), four quaternary carbons ($\delta_C$ 107.0, 144.1, 165.4 and 165.9), four olefinic methines ($\delta_C$ 99.7, 102.6, 111.6 and 142.7), four oxymethines ($\delta_C$ 71.3, 75.7, 86.4 and 90.7), one oxymethylene ($\delta_C$ 62.3), a methoxy unit ($\delta_C$ 55.8) and a methyl group ($\delta_C$ 24.1). Its $^1H$ NMR data (Table 1) indicated the presence of a 1,2,3,5-tetrasubstituted benzene ring ($\delta_H$ 6.31 and 6.33), a methyl group ($\delta_H$ 2.48, s) and a methoxy group ($\delta_H$ 3.79, s). These data suggested that the structure of **5** was highly similar to that of the co-isolated known compound kipukasin D (**7**) [22], with the primary difference in the resonance at C-2′, C-3′, C-4′, C-7′ and the benzene ring. However, comprehensive analysis of 2D NMR of **5** indicated the presence of a hydroxyl group attached at C-2″ in **5** instead of a methoxy group in **7**, which was unambiguously confirmed by single-crystal X-ray diffraction experiments (Fig. 6). The conformation of compound **5** differed from that of **7** in the X-ray diffraction experiments, resulting in significant chemical shift discrepancies in ribose and 1,2,3,5-tetrasubstituted benzene ring moieties (Fig. 7).

The mixed $^{13}C$ NMR data of the minor component (**6**) (Table 2) exhibited similarities to the co-isolated compound (**5**) [22], with the primary differences observed at C-1′, C-2′, and C-3′, as evidenced by the resonance at these positions. The structure of **6** was elucidated through $^1H$–$^1H$ COSY cross-peaks observed between H-1′/H-2′/H-3′/H-4′/H-5′ and HMBC correlation from H-2′ to H-7″, confirming it as a regioisomer of **5** (Fig. S1).

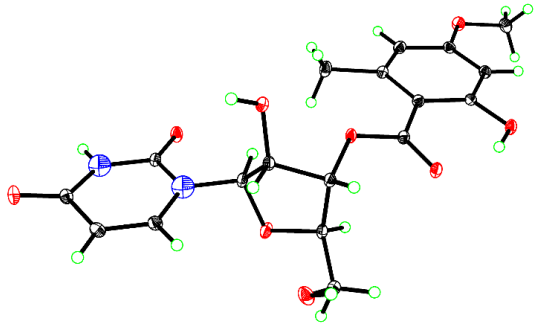

**Fig. 6** X-ray crystallographic structure of **5**.

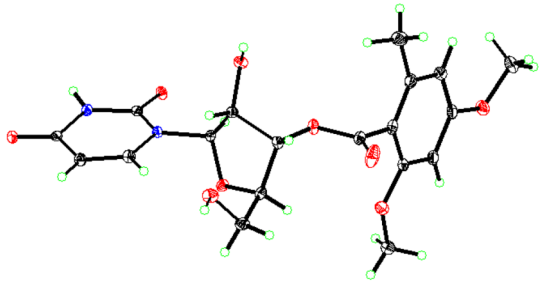

**Fig. 7** X-ray crystallographic structure of **7**.

The absolute configuration of **5** was subsequently determined through single-crystal X-ray diffraction analysis (Fig. 6). After numerous attempts with various solvent systems, a suitable crystal was successfully obtained from a methanol (MeOH)/water mixture (10∶1). This crystal underwent single-crystal X-ray diffraction testing, which conclusively identified its absolute configuration as 1′*R*,2′*R*,3′*S*,4′*R* [Flack parameter = 0.12(7); Cambridge Crystallographic Data Centre (CCDC) 2286888]. Furthermore, given that **6** is a regioisomer of **5** and shares a common biogenesis, the stereochemical structure of **6** was also confirmed.

TNF-α is a pleiotropic cytokine that plays crucial roles in autoimmune disorders, including rheumatoid arthritis (RA), psoriatic arthritis, multiple sclerosis, and Crohn's disease [23, 24]. Consequently, direct inhibition of TNF-α has emerged as a primary therapeutic approach for treating these conditions. Compounds **1**–**8** were assessed for their TNF-α inhibitory activities *in vitro*. As illustrated in Table 3, compounds **1** and **2** demonstrated the most potent TNF-α inhibitory activities, with $IC_{50}$ values of (9.24 ± 0.78) and (8.95 ± 0.62) $\mu mol \cdot L^{-1}$, respectively.

To further elucidate their mechanisms of action, the binding modes and energies of compounds **1**, **2**, **5**, **6**, **7**, and **8** with TNF-α dimer were determined through molecular docking. As depicted in Fig. 8, the binding pocket of the TNF-α dimer is relatively spacious and featureless. Compounds **1** and **2** effectively occupied the binding site of the crystallographic ligand SPD304, potentially inhibiting the binding of the third subunit that forms a biologically active trimer complex. Compound **1** established several hydrophobic interactions with LEU57, TYR59, TYR119, GLY121, and TYR151 from both TNF-α monomers. Notably, the benzyl groups in **1** exhibit strong π–π interactions with the residues of TYR59 and GLY121, which play a crucial role in stabilizing the binding with the ligands.

This study represents the initial documentation of nucleosides functioning as TNF-α inhibitors, potentially offering novel

**Table 3** TNF-$\alpha$ inhibitory activities of compounds **1**–**8**.

| No. | $IC_{50}$/($\mu mol \cdot L^{-1}$) Treated with TNF-α | $IC_{50}$/($\mu mol \cdot L^{-1}$) Untreated with TNF-α | Total score |
|---|---|---|---|
| **1** | 9.24 ± 0.78 | > 40 | 5.8201 |
| **2** | 8.95 ± 0.62 | > 40 | 5.2017 |
| **3/4** | > 20 | > 40 | 6.4210/5.7795 |
| **5/6** | 15.50 ± 1.30 | > 40 | 5.2270/4.5189 |
| **7/8** | 17.70 ± 1.40 | > 40 | 3.9848/6.6027 |
| SPD304 | 4.99 ± 0.52 | > 40 | −32.900 |

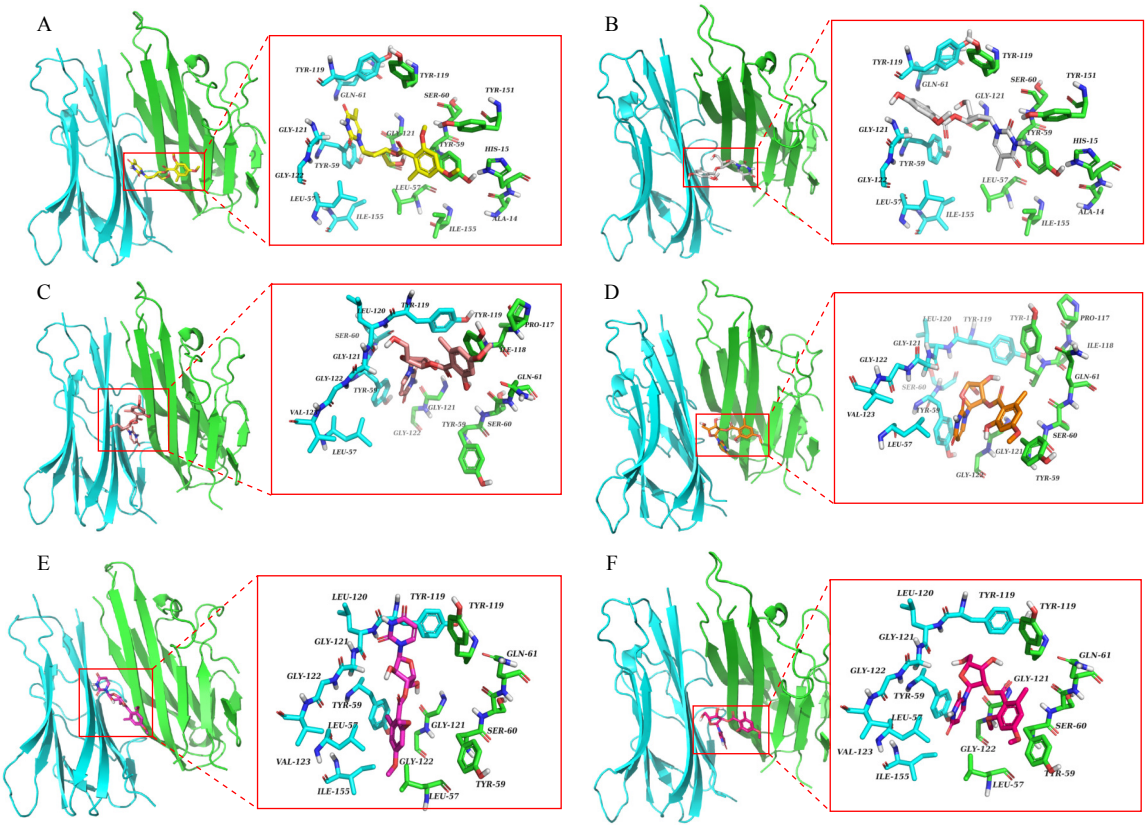


**Fig. 8** The binding modes and energies of compounds **1**, **2** and **5**–**8** (A: **1**; B: **2**; C: **5**; D: **6**; E: **7**; F: **8**).

chemical structures for the development of therapeutic agents targeting autoimmune and inflammatory disorders.

## 3. Conclusion

In conclusion, this study identified and characterized six novel nucleoside derivatives from *Aspergillus amoenus* TJ507. The structural elucidation was accomplished through a combination of spectroscopic analysis, single-crystal X-ray crystallography, ECD calculations, and chemical reactions. Notably, 2′/3′-transesterification reactions were observed between compounds **3**/**4**, **5**/**6**, and **7**/**8**. Compounds **3** and **4** are significant as they represent the first reported nucleoside derivatives incorporating a pyrrole moiety. Furthermore, compounds **1**, **2**, and **5**–**8** demonstrated moderate TNF-α inhibitory activities. This research contributes to the expanding repertoire of fungal-derived nucleoside derivatives and presents a potential chemical framework for addressing autoimmune diseases and inflammation.

## 4. Experimental

### 4.1. General experimental procedures

NMR data were obtained using Bruker AM-400 and AV-600 spectrometers (Bruker, Karlsruhe, Germany). High-resolution electrospray ionization mass spectrometry (HR-ESI-MS) data were collected using a SolariX 7.0 T Bruker Daltonics system (Bruker, Karlsruhe, Germany). UV spectra were recorded on a Lambda 35 instrument (PerkinElmer Inc., Fremont, California, USA). Optical rotations and ECD data were measured using a PerkinElmer 341 Polarimeter (Rudolph Research Analytical, Hackettstown, NJ, USA) and a JASCO-810 spectrometer (JASCO)-810 spectrometer (JASCO, Tokyo, Japan), respectively. Fourier-transform infrared (FT-IR) spectra were acquired using a Bruker Vertex 70 instrument (Bruker, Karlsruhe, Germany). Crystallographic experiments were conducted using a Bruker SMART APEX-II CCD diffractometer with graphite-monochromated Cu-Kα radiation (Bruker, Karlsruhe, Germany). Column chromatography (CC) was performed for sample separation using silica gel (200–300 and 100–200 mesh; Qingdao Marine Chemical Inc., China), ODS (50 μm, YMC Co., Ltd., Japan, as stationary phase), and Sephadex LH-20 (Pharmacia Biotech AB, Uppsala, Sweden). Semipreparative HPLC was conducted using an Agilent 1200 system with an RP $C_{18}$ column (5 μm, 10 mm × 250 mm, Welch Ultimate XB-$C_{18}$), while analytical HPLC was performed on a Dionex HPLC system.

### 4.2. Fungal material

*Aspergillus amoenus* TJ507 was isolated from fresh leaves of *Hypericum wilsonii* N. Robson, collected in the Shennongjia District, China. The fungus was identified through morphological examination and sequence analysis of the ITS region of rDNA (GenBank accession No. OQ626373). A voucher specimen of the isolated fungus has been deposited at the culture collection center of Tongji Medical College, Huazhong University of Science and Technology, under the accession number TJ20210512556.

### 4.3. Fermentation, extraction and isolation

The strain *Aspergillus amoenus* TJ507 was cultured on potato dextrose agar (PDA) plates at 28 °C for 4 d. Subsequently, the agar was used to inoculate 400 Erlenmeyer flasks (1 L), each containing 250 g of rice and 200 mL of distilled water. All flasks were incubated at 28 °C for 32 d. The solid cultures were then subjected to ten extractions with 95% aqueous EtOH at room temperature and subsequently evaporated under vacuum to obtain a total residue. This residue was suspended in water and fully partitioned with ethyl acetate (EtOAc) twelve times at room temperat-

ure. The total EtOAc extract (1.5 kg) was fractionated into six fractions (Fr.1–Fr.6) using silica gel CC with an increasing gradient of PE∶EtOAc∶methanol (50∶1∶0–1∶1∶1). Fraction 2 (200 g) underwent further fractionation on an octadecylsilyl reversed phase chromatography $C_{18}$ (ODS RP-$C_{18}$) column using a mixture of MeOH and $H_2O$ (20∶80–80∶20) as the eluent, resulting in seven fractions (Fr.2.1–Fr.2.7). Fr.2.3 was subsequently purified using silica gel $CH_2Cl_2$∶MeOH (100∶1–1∶1), followed by further purification using Sephadex LH-20 CC (MeOH∶$CH_2Cl_2$, 1∶1). Finally, these fractions were purified by semipreparative high-performance liquid chromatography (HPLC) (2.0 mL·min$^{-1}$, 210 nm) to obtain **5** and **6** (4 mg; $CH_3CN$∶$H_2O$, 30∶70, *V/V*, $t_R$ = 20 min), **3** and **4** (3 mg; $CH_3CN$∶$H_2O$, 44∶56, *V/V*, $t_R$ = 18 min), **2** (3 mg; $CH_3CN$∶$H_2O$, 33∶66, *V/V*, $t_R$ = 24 min), **7** and **8** (100 mg; $CH_3OH$∶$H_2O$, 53∶47, *V/V*, $t_R$ = 15 min). Additionally, Fr.2.4 was loaded onto silica gel CC (200–300 mesh) with a gradient elution of $CH_2Cl_2$∶MeOH (100∶1–1∶1), then applied to Sephadex LH-20 eluted with $CH_2Cl_2$∶MeOH (1∶1) and repeatedly purified by RP-HPLC (2.0 mL·min$^{-1}$, 210 nm) to yield **1** (7.0 mg; $CH_3CN$∶MeOH, 40∶60, *V/V*, $t_R$ = 29 min).

Amoenucle A (**1**): colorless oil; $[\alpha]_D^{25}$ −54 (*c* 0.1, MeOH); IR $\nu_{max}$ 3431, 1698, 1604, 1469, 1267, 1161, and 1096 cm$^{-1}$; UV (MeOH) $\lambda_{max}$ (log $\varepsilon$) 201 (4.51) nm; ECD (MeOH) $\lambda_{max}$ ($\Delta\varepsilon$) 221 (−3.08), 267 (+1.29) nm; for $^1$H NMR (400 MHz) and $^{13}$C NMR (100 MHz) data (Tables 1 and 2); HR-ESI-MS [M + Na]$^+$ *m/z* 443.1463 (Calcd. for $C_{20}H_{24}N_2O_8Na$, 443.1430).

Amoenucle B (**2**): colorless oil; $[\alpha]_D^{25}$ −36 (*c* 0.1, MeOH); IR $\nu_{max}$ 3431, 1698, 1607, 1472, 1266, 1166 and 1093 cm$^{-1}$; UV (MeOH) $\lambda_{max}$ (log $\varepsilon$) 201 (4.48) nm; ECD (MeOH) $\lambda_{max}$ ($\Delta\varepsilon$) 222 (−3.03), 267 (+1.24) nm; for $^1$H NMR (400 MHz) and $^{13}$C NMR (100 MHz) data (Tables 1 and 2); HR-ESI-MS [M + Na]$^+$ *m/z* 429.1274 (Calcd. for $C_{19}H_{22}N_2O_8Na$, 429.1261).

Amoenucles C and D (**3/4**): colorless oil; $[\alpha]_D^{25}$ −57 (*c* 0.1, MeOH); IR $\nu_{max}$ 3396, 2921, 1693, 1646, 1595, 1468, 1325, 1261, 1157, 1081, 815 and 771 cm$^{-1}$; UV (MeOH) $\lambda_{max}$ (log $\varepsilon$) 204 (4.58) nm; ECD (MeOH) $\lambda_{max}$ ($\Delta\varepsilon$) 203 (+16.71), 213 (−1.81), 246 (−2.09)nm, 273 (+0.70) nm; for $^1$H NMR (600 MHz) and $^{13}$C NMR (150 MHz) data (Tables 1 and 2); HR-ESI-MS [M + Na]$^+$ *m/z* 552.1609 (Calcd. for $C_{25}H_{27}N_3O_{10}Na$, 552.1594).

Amoenucle E (**5**): colorless crystal; $[\alpha]_D^{25}$ −15 (*c* 0.1, MeOH); IR $\nu_{max}$ 3426, 1690, 1468, 1270, 1106 and 1055 cm$^{-1}$; UV (MeOH) $\lambda_{max}$ (log $\varepsilon$) 212 (4.41) nm; ECD (MeOH) $\lambda_{max}$ ($\Delta\varepsilon$) 228 (+1.76), 272 (−2.69) nm; for $^1$H NMR (600 MHz) and $^{13}$C NMR (150 MHz) data (Tables 1 and 2); HR-ESI-MS [M + Na]$^+$ *m/z* 431.1050 (Calcd. for $C_{18}H_{20}N_2O_9Na$, 431.1066).

### 4.4. Alkaline hydrolysis reaction

Compounds **1** (2.19 mg), **2** (1.14 mg), and **3/4** (1.84 mg) were dissolved in 1 mL MeOH and treated with 0.01 g NaOH, stirring at room temperature for 48 h. Thin-layer chromatography (TLC) was used to monitor the reaction progress. Subsequently, the reaction solution of **1** was evaporated under vacuum and purified by reversed-phase high-performance liquid chromatography (RP-HPLC) using $H_2O$–MeOH (17∶83) with diode array detection (DAD) to obtain **1a** (1.55 mg). Similarly, **2a** (1.12 mg) and **3a** (1.07 mg) were obtained from the hydrolysis products of **2** and **3/4**, respectively. Additionally, the retention times of uracil-1-*β*-D-ribofuranoside (CAS: 58-96-8, Yuanye, China) and thymine-1-*β*-D-deoxyribofuranoside (CAS: 50-89-5, Yuanye, China) were determined by RP-HPLC under identical conditions. The results indicated that the retention times of **1a** and **2a** were identical to thymine-1-*β*-D-deoxyribofuranoside, while the retention time of **3a** matched that of uracil-1-*β*-D-ribofuranoside. Moreover, circular dichroism (CD) spectra of the hydrolysates were compared to standards, revealing consistent trends. Consequently, the nucleoside portions of the compounds were confirmed by comparing the retention times and CD spectra of the reaction products with those of reference standards.

### 4.5. Theoretical ECD calculation

Conformational analyses were conducted *via* random searching in Sybyl-X 2.0 using the MMFF94S force field. The ECD spectra of each conformer were calculated using the TD-DFT methodology at the PBE0/def2-TZVP level in CPCM methanol using the ORCA 5.0.1 program. The ECD spectra were simulated using an overlapping Gaussian function. Based on the population contributions of the spectra, Boltzmann weighting was applied, and a UV correction was implemented.

### 4.6. X-ray crystal structure analysis

The crystallographic data for compounds **5** and **7** were deposited in the CCDC under Supplementary Publication No. 2286888 and 2304831, respectively.

Crystallographic data of amoenucle E (**5**): $C_{18}H_{20}N_2O_9$, $M$ = 408.36, $a$ = 6.466 90(10) Å, $b$ = 7.521 90(10) Å, $c$ = 9.458 20(10) Å, $\alpha$ = 98.1370(10) °, $\beta$ = 104.1630(10) °, $\gamma$ = 91.0450(10) °, $V$ = 440.932(10) Å$^3$, $T$ = 293(2) K, space group $P1$, $Z$ = 1, μ(Cu Kα) = 1.069 mm$^{-1}$, 8123 reflections measured, 3293 independent reflections ($R_{int}$ = 0.0179). The final $R_1$ values were 0.0286 [I > 2$\sigma$(*I*)]. The final w$R(F^2)$ values were 0.0778 [I > 2$\sigma$(*I*)]. The final $R_1$ values were 0.0287 (all data). The final w$R(F^2)$ values were 0.0780 (all data). The goodness of fit on $F^2$ was 1.055. The Flack parameter was determined to be 0.12(7).

Crystallographic data of kipukasin D (**7**): $C_{19}H_{22}N_2O_9$, $M$ = 422.38, $a$ = 11.885 70(10) Å, $b$ = 6.919 Å, $c$ = 23.677 00(10) Å, $\alpha$ = 90 °, $\beta$ = 94.24 °, $\gamma$ = 90 °, $V$ = 1941.810(18) Å$^3$, $T$ = 293(2) K, space group $P2_1$, Z = 4, μ(Cu Kα) = 0.990 mm$^{-1}$, 44360 reflections measured, 7599 independent reflections ($R_{int}$ = 0.0314). The final $R_1$ values were 0.0324 [I > 2$\sigma$(*I*)]. The final w$R(F^2)$ values were 0.0843 [I > 2$\sigma$(*I*)]. The final $R_1$ values were 0.0326 (all data). The final w$R(F^2)$ values were 0.0844 (all data). The goodness of fit on $F^2$ was 1.047. Flack parameter = −0.02(3).

### 4.7. Evaluation of the cellular susceptibility to TNF-α

L929 cells were obtained from Procell Life Science & Technology Co., Ltd. (Wuhan, China). The cells were cultured in RPMI-1640 medium supplemented with 10% fetal bovine serum (FBS) and 1% penicillin/streptomycin (Gibco, CA, USA). The culture conditions were maintained at 37 °C in a humidified incubator with 95% air and 5% $CO_2$. The cytotoxicity assessment on L929 cells was conducted using the cell counting kit-8 (CCK8) method, following previously described protocols with minor modifications.

In this experiment, the cytotoxicity of compounds towards L929 cells was evaluated using the CCK8 method. Additionally, 2.0 ng·mL$^{-1}$ TNF-α was incubated with varying concentrations of compounds for 2 h at 37 °C in a 96-well plate before the introduction of 1 × 10$^5$ L929 cells/mL to assess the selected compounds' ability to neutralize human TNF-α bioactivity in L929 cells. The assay mixture, with a total volume of 100 μL, was incubated at 37 °C for 24 h. The inhibition rate of L929 cell proliferation was determined using a colorimetric assay employing the CCK8 method. $IC_{50}$ values were calculated using the Reed–Muench method [25-29].

### 4.8. Virtual docking

The binding affinity of the compounds with TNF-α was assessed through molecular docking studies using the Surflex-Dock module of the FlexX/Sybyl software. The 3D crystal structure of

TNF-α (PDB ID: 2AZ5) with a resolution of 2.10 Å was obtained from the RCSB Protein Data Bank (http://www.rcsb.org) [25]. The crystallographic ligand was removed from the active site, and the designed ligands were modeled. Protein preparation involved the removal of all water molecules and other ligand structures, followed by the addition of missing hydrogens. The 3D structures of the compounds were created using ChemDraw 3D software. Molecular docking was conducted using the CDOCKER protocol to analyze the binding affinities between the ligands and the protein. In the docking calculations, the default FlexX scoring function was employed for exhaustive searching, solid body optimization, and interaction scoring. Subsequently, the ligands with the lowest energy and most favorable orientation were selected [30].

## Funding

This research was supported by the National Natural Science Foundation for Distinguished Young Scholars (No. 81725021) and the National Natural Science Foundation of China (Nos. 82003633 and 82173705).

## Declaration of competing interest

These authors have no conflict of interest to declare.

## Supplementary material

Supplementary material related to this article can be requested by sending E-mails to the corresponding authors.

## References

1 Chien M, Anderson TK, Jockusch S, et al. Nucleotide analogues as inhibitors of SARS-CoV-2 polymerase, a key drug target for COVID-19. *J Proteome Res*. 2020;19(11):4690–4697. https://doi.org/10.1021/acs.jproteome.0c00392.
2 Curtis BJ, Schwertfeger TJ, Burkhardt RN, et al. Oligonucleotide catabolism-derived gluconucleosides in caenorhabditis elegans. *J Am Chem Soc*. 2023;145 (21):11611–11621. https://doi.org/10.1021/jacs.3c01151.
3 Jordheim LP, Durantel D, Zoulim F, et al. Advances in the development of nucleoside and nucleotide analogues for cancer and viral diseases. *Nat Rev Drug Discov*. 2013;12(6):447–464. https://doi.org/10.1038/nrd4010.
4 Shelton J, Lu X, Hollenbaugh JA, et al. Metabolism, biochemical actions, and chemical synthesis of anticancer nucleosides, nucleotides, and base analogs. *Chem Rev*. 2016;116(23):14379–14455. https://doi.org/10.1021/acs.chemrev.6b00209.
5 Abbas M, Elshahawi SI, Wang X, et al. Puromycins B–E, naturally occurring amino-nucleosides produced by the himalayan isolate *Streptomyces* sp. PU-14G. *J Nat Prod*. 2018;81(11):2560–2566. https://doi.org/10.1021/acs.jnatprod.8b00720.
6 Bracegirdle J, Gordon DP, Harvey JE, et al. Kinase-inhibitory nucleoside derivatives from the pacific bryozoan *Nelliella nelliiformis*. *J Nat Prod*. 2020;83 (2):547–551. https://doi.org/10.1021/acs.jnatprod.9b01231.
7 Maffioli SI, Zhang Y, Degen D, et al. Antibacterial nucleoside-analog inhibitor of bacterial RNA polymerase. *Cell*. 2017;169(7):1240–1248. https://doi.org/10.1016/j.cell.2017.05.042.
8 Rossiter SE, Fletcher MH, Wuest WM. Natural products as platforms to overcome antibiotic resistance. *Chem Rev*. 2017;117(19):12415–12474. https://doi.org/10.1021/acs.chemrev.7b00283.
9 Zafrir IE, Torres MR, Prudhomme J, et al. Farnesides A and B, sesquiterpenoid nucleoside ehers from a marine-derived *Streptomyces* sp. strain CNT-372 from *Fiji*. *J Nat Prod*. 2013;76(9):1815–1818. https://doi.org/10.1021/np400351t.
10 Murakami R, Fujita Y, Kizuka M, et al. A-94964, a novel inhibitor of bacterial translocase I, produced by *Streptomyces* sp. SANK 60404. *J Antibiot*. 2008;61 (9):537–544. https://doi.org/10.1038/ja.2008.71.
11 Robinson FA. Chemistry of penicillin. *Analyst*. 1947;72(856):274–276. https://doi.org/10.1039/an9477200274.
12 Evidente A, Kornienko A, Cimmino A, et al. Fungal metabolites with anticancer activity. *Nat Prod Rep*. 2014;31(5):617–627. https://doi.org/10.1039/C3NP70078J.
13 Xu QS, Zhu HJ, Sun ZQ, et al. Lysohexaenetides A and B, linear lipopeptides from *Lysobacter* sp. DSM 3655 identified by heterologous expression in *Streptomyces*. *Chin J Nat Med*. 2023;21(6):454–458. https://doi.org/10.1016/S1875-5364(23)60473-X.
14 Krukemyer JJ. Lovastatin: a new cholesterol-lowering agent. *Pharmacotherapy*. 1987;7(6):198–210. https://doi.org/10.1002/j.1875-9114.1987.tb03524.x.
15 Liu N, Song MN, Zhang QQ, et al. GKK1032B from endophytic *Penicillium citrinum* induces the apoptosis of human osteosarcoma MG63 cells through caspase pathway activation. *Chin J Nat Med*. 2022;20(1):67–73. https://doi.org/10.1016/S1875-5364(21)60108-5.
16 Salman K, Zhu H, Sun Z, et al. Seven drimane-type sesquiterpenoids from an earwig-associated *Aspergillus* sp.. *Chin J Nat Med*. 2023;21(1):58–64. https://doi.org/10.1016/S1875-5364(23)60385-1.
17 Deng M, Chen X, Qiao Y, et al. Isolation, absolute configurations and bioactivities of pestaphilones A–I: undescribed methylated side chain containing-azaphilones from *Pestalotiopsis oxyanthi*. *Phytochemistry*. 2022; 194:113045. https://doi.org/10.1016/j.phytochem.2021.113045.
18 Hu H, Li Y, Shi Z, et al. Discovery of ergosterol derivative from *Aspergillus* sp. TJ507 that protects against hepatic ischemia/reperfusion injury. *Bioorg Chem*. 2023;135:106530. https://doi.org/10.1016/j.bioorg.2023.106530.
19 Qi C, Bao J, Wang J, et al. Asperterpenes A and B, two unprecedented meroterpenoids from *Aspergillus terreus* with BACE1 inhibitory activities. *Chem Sci*. 2016;7(10):6563–6572. https://doi.org/10.1039/C6SC02464E.
20 Qiao Y, Xu Q, Feng W, et al. Asperpyridone A: an unusual pyridone alkaloid exerts hypoglycemic activity through the insulin signaling pathway. *J Nat Prod*. 2019;82(10):2925–2930. https://doi.org/10.1021/acs.jnatprod.9b00188.
21 Zhang Y, Zhao X, Cao Y, et al. Bioactive indole alkaloid from *Aspergillus amoenus* TJ507 that ameliorates hepatic ischemia/reperfusion injury. *J Nat Prod*. 2023;86(8):2059–2064. https://doi.org/10.1021/acs.jnatprod.3c00251.
22 Jiao P, Mudur SV, Gloer JB, et al. Kipukasins, nucleoside derivatives from *Aspergillus versicolor*. *J Nat Prod*. 2007;70(8):1308–1311. https://doi.org/10.1021/np070241l.
23 Sethi JK, Hotamisligil GS. Metabolic messengers: tumour necrosis factor. *Nat Metab*. 2021;3(10):1302–1312. https://doi.org/10.1038/s42255-021-00470-z.
24 Jang DI, Lee AH, Shin HY, et al. The role of tumor necrosis factor alpha (TNF-α) in autoimmune disease and current TNF-α inhibitors in therapeutics. *Int J Mol Sci*. 2021;22(5):2719. https://doi.org/10.3390/ijms22052719.
25 He MM, Smith AS, Oslob JD, et al. Small-molecule inhibition of TNF-α. *Science*. 2005;310(5750):1022–1025. https://doi.org/10.1126/science.1116304.
26 Javaid N, Patra MC, Cho DE, et al. An orally active, small-molecule TNF inhibitor that disrupts the homotrimerization interface improves inflammatory arthritis in mice. *Sci Signal*. 2022;15(759):eabi8713. https://doi.org/10.1126/scisignal.abi8713.
27 Lai X, Wei J, Ding X. Paeoniflorin antagonizes TNF-α-induced L929 fibroblastoma cells apoptosis by inhibiting NF-κB p65 activation. *Dose Response*. 2018;16(2):1559325818774977. https://doi.org/10.1177/1559325818774977.
28 Sun W, Wu Y, Zheng M, et al. Discovery of an orally active small-molecule tumor necrosis factor-α inhibitor. *J Med Chem*. 2020;63(15):8146–8156. https://doi.org/10.1021/acs.jmedchem.0c00377.
29 Sawai H. Induction of apoptosis in TNF-α treated L929 cells in the presence of necrostatin-1. *Int J Mol Sci*. 2016;17(10):1678. https://doi.org/10.3390/ijms17101678.
30 Zang Y, Gong YH, Li XW, et al. Canescones A–E: aromatic polyketide dimers with PTP1B inhibitory activity from *Penicillium canescens*. *Org Chem Front*. 2019;6(18):3274–3281. https://doi.org/10.1039/C9QO00820A.